Two-Dimensional Exponential Chaotic System With Hardware Implementation

Yinxing Zhang, Han Bao ⬥, *Member, IEEE*, Zhongyun Hua ⬥, *Member, IEEE,* and Hejiao Huang ⬥

Abstract—**Recently, designing hyperchaotic maps with complex dynamics has attracted increasing attention from various research fields. In this article, we propose a 2-D exponential chaotic system (2D-ECS). The 2D-ECS can generate a large number of hyperchaotic maps by cascading exponential nonlinearity with bounded functions. To show the effectiveness of the 2D-ECS, we provide three hyperchaotic maps by cascading the exponential nonlinearity with trigonometric functions. We first build state-mapping networks with different fixed-point arithmetic precisions to analyze the dynamic properties of the hyperchaotic maps in digital domain, and then study their dynamic properties using several numerical measurements. Experimental results show that the generated hyperchaotic maps show better performance indicators than existing chaotic maps. Moreover, a hardware platform is constructed to implement the three hyperchaotic maps generated by the 2D-ECS, and two-channel hyperchaotic sequences are experimentally captured. A pseudorandom number generator is designed to study the potential applications of our proposed hyperchaotic maps. Finally, we apply the generated hyperchaotic maps to secure communication, and experimental results show that these maps exhibit better performance in contrast to existing chaotic maps.**

Index Terms—**Fixed-point arithmetic, hardware implementation, hyperchaotic map, period distribution, pseudorandom number generator (PRNG), state-mapping network.**

Yinxing Zhang is with the School of Computer Science and Technology, Harbin Institute of Technology, Shenzhen 518055, China (e-mail: 19b951006@stu.hit.edu.cn).

Han Bao is with the School of Microelectronics and Control Engineering, Changzhou University, Changzhou 213164, China (e-mail: hanbao@cczu.edu.cn).

Zhongyun Hua and Hejiao Huang are with Guangdong Provincial Key Laboratory of Novel Security Intelligence Technologies, the School of Computer Science and Technology, Harbin Institute of Technology, Shenzhen 518055, China (e-mail: huazyum@gmail.com; huazhongyun@hit.edu.cn; huanghejiao@hit.edu.cn).

I. INTRODUCTION

IN THE past few decades, nonlinear system has attracted increasing attention of researchers from many disciplines [1], [2] and has been extensively applied in various industrial fields [3], [4]. Chaotic systems, as a class of nonlinear systems, are mathematical models to describe chaotic behaviors [5]. When the initial value of a chaotic system is known, the system is deterministic. On the contrary, if its initial value is unknown, its trajectories cannot be accurately predicted. With this characteristic, a chaotic system can achieve many unique properties, such as the density of periodic orbits, track ergodicity, and initial condition sensitivity [6]. Such valuable properties make the chaotic systems suitable for many applications in the fields of electrical engineering and computer science [7], [8]. Especially, chaotic systems exhibit outstanding performance in secure communication and pseudorandom number generator (PRNG) [9], [10], [11].

When applying a chaotic system to practical applications, researchers discovered that chaotic systems without high complexity may result in many serious problems [12]. First, chaotic systems with low complexity can easily happen dynamic degradation when they are simulated on a digitalized platform [13]. Once chaos degradation occurs, many chaos-based applications become ineffective. For example, the chaos-based cryptosystems are vulnerable to security attacks if their used chaotic systems occur chaos degradation [14]. Second, with the rapid development of artificial intelligence technologies, chaotic trajectories of many existing chaotic systems can be exactly deduced from a little data [15]. The researchers may estimate the chaotic behaviors of a chaotic system by directly predicting its chaotic trajectories or estimating its control parameters [16]. If the chaotic behaviors can be successfully detected, a chaotic system loses the characteristic of unpredictability, and thereby its corresponding applications may also become ineffective [17]. Therefore, it is of critical importance to design chaotic systems owning complex behaviors to against chaos degradation and chaotic behavior prediction.

A hyperchaotic system usually shows complex behaviors and, thus, is more suitable for many chaos-based applications [18]. A dynamic system with two or more positive Lyapunov exponents (LEs) can produce hyperchaotic behaviors, whereas with one LE can only produce normal chaotic behaviors. Generally speaking, a chaotic system with more dimensions owns more complex dynamic behaviors, and its trajectories are harder to predict, but it also requires more time to implement [10]. Besides, to produce

hyperchaotic behaviors, a continuous chaotic system requires at least four dimensions, whereas a discrete chaotic map requires only two [19]. When being simulated in a real system, a continuous system should be discretized using some discretization algorithms, which may be time-consuming. In addition, when applying a chaotic system to some practicalities, such as secure communication, only one or two chaotic sequences are required. Thus, these practicalities usually use low-dimensional chaotic systems as chaos generators [20], because high-dimensional (HD) chaotic systems can generate multiple chaotic sequences, which is a waste of computation cost. Therefore, constructing 2-D discrete chaotic maps with complex hyperchaotic behaviors is significant. However, except for a few specially designed ones [12], [21], most 2-D discrete chaotic maps have only one positive LE and cannot show hyperchaotic behaviors [22], [23].

In the past few years, researchers have developed some 2-D hyperchaotic maps with complex dynamics properties. Several representative examples are listed as follows. Kong et al. [21] applied the trigonometric nonlinearity as a controller to a 2-D discrete linear map and obtained a hyperchaotic map. Li et al. [20] developed four 2-D memristive discrete maps by coupling a discrete cosine memristor model into 1-D discrete maps. Recently, a 2-D hyperchaotic map is proposed in [19] to exhibit hyperchaotic behaviors by coupling the logistic map with a special nonlinear term. Most of these methods generate hyperchaotic maps by expanding the systems from 1-D to 2-D using different nonlinearity, and this strategy may cause low complexity to the generated hyperchaotic sequences. In addition, many 2-D chaotic maps [19], [22], [24] have quite narrow and discontinuous chaotic ranges because their phase planes will become uncompacted as their control parameters increase. All digital platforms have finite precision. When a chaotic system is implemented on digital platforms, its digitalized parameter(s) can only achieve approximate values. If the chaotic ranges are discontinuous, a slight disturbance to the parameters may result in the parameter(s) without chaotic ranges, leading to chaotic behaviors degrading to regular behaviors. This also causes serious adverse effects in many chaos-based practical applications. Consequently, designing new 2-D discrete hyperchaotic maps with higher complexity and larger chaotic ranges is significant.

This article presents a 2-D exponential chaotic system (2D-ECS) to generate 2-D hyperchaotic maps with complex chaotic behaviors. 2D-ECS has a simple structure and can generate many 2-D discrete hyperchaotic maps by cascading exponential nonlinearity with some bounded functions. 2D-ECS uses a bounded function to ensure that the phase plane of the system is always compacted, and thus, the generated chaotic maps have large and continuous chaotic ranges. The main contributions of this work are summarized in the following.

1) We propose 2D-ECS, a general framework of producing 2-D hyperchaotic maps by cascading exponential nonlinearity with bounded functions. We also create three examples of new 2-D hyperchaotic maps to show the effectiveness of 2D-ECS.
2) We build state-mapping networks under different precisions to show the dynamic properties of the new chaotic maps in digital domain. We also evaluate the new chaotic
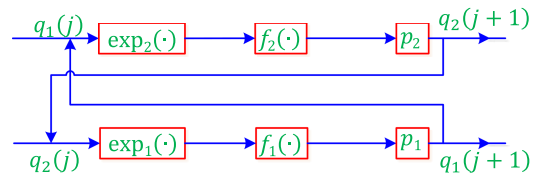

Fig. 1. Structure of the 2D-ECS.

maps using different indicators, and the results show that they can achieve better performance indicators than representative 2-D chaotic maps.

3) We simulate the new chaotic maps on a microcontroller-based hardware platform and test their captured hyperchaotic sequences using a strict random number test standard. The test results show that the new chaotic maps can generate chaotic sequences with high randomness in contrast to existing 2-D chaotic maps.
4) We apply the new chaotic maps to secure communication to demonstrate its practicality. The experimental results show that these chaotic maps exhibit better performance in resisting transmission noise in this application than existing chaotic maps.

The rest of this article is organized as follows. Section II provides the 2D-ECS and its generated 2-D hyperchaotic maps. Section III builds state-mapping networks to explore the dynamic behaviors of the generated 2-D hyperchaotic map in digital domain. Section IV analyzes the chaotic behaviors of the three 2-D hyperchaotic maps and compares their performance indicators with other chaotic maps. Section V builds a hardware experiment and applies the three 2-D hyperchaotic maps to the applications of PRNG and secure communication. Finally, Section VI concludes this article.

II. 2-D EXPONENTIAL CHAOTIC SYSTEM

This section presents the 2D-ECS. To show its effectiveness, three examples of 2-D hyperchaotic maps are constructed and the stability of their fixed points (FPs) is analyzed.

A. Definition of 2D-ECS

The 2D-ECS is designed by cascading exponential nonlinearity with bounded functions, and its structure is shown in Fig. 1. As can be seen, the top branch describes the iteration process, in which the variable $q_1(j)$ is fed into the input of the exponential function $\exp_1(\cdot)$, and then, the output of $\exp_1(\cdot)$ is fed into the input of function $f_1(\cdot)$. After multiplying with a parameter p_1, the obtained output is used as the input of the bottom branch, where the bottom branch performs the same process with the top branch. When the exponential functions $\exp_1(\cdot)$ and $\exp_2(\cdot)$ are both set to $\exp(q^2)$, the mathematical form of the 2D-ECS can be described by

$$\begin{cases} q_1(j+1) = p_1 f_1 \left(\exp \left(q_2^2(j) \right) \right) \\ q_2(j+1) = p_2 f_2 \left(\exp \left(q_1^2(j) \right) \right) \end{cases} \tag{1}$$

where p_1 and p_2 are two control parameters, and f_1 and f_2 are two bounded functions.

The output of an exponential function diverges and may tend to infinity. However, a bounded function can ensure that the output is within a fixed range. By cascading the exponential function with bounded functions, the 2D-ECS can show the chaos properties. The 2D-ECS provides users great flexibility to produce a large number of hyperchaotic maps by using different exponential functions and different bounded functions. Moreover, each branch of the 2D-ECS structure in Fig. 1 can be further expanded to cascade three or more functions. This provides more flexibility for users to choose more functions in the construction process. The generated hyperchaotic maps may possess more control parameters and more hyperchaotic behaviors, which can generate better hyperchaotic performance indicators and unpredictable hyperchaotic sequences compared with existing hyperchaotic maps. These will be verified by experimental analysis in Section IV. However, some chaos-based applications need only one chaotic sequence while our 2-D chaotic maps produce two chaotic sequences. This may lead to an extra computation cost. Each output state of the new hyperchaotic map is a floating-point number. When designing PRNG using the output states, we use only several bits for each output state and discard the rest bits. This may cause a reduction of efficiency.

B. Examples of 2-D Hyperchaotic Maps

To show the effectiveness of the 2D-ECS, we provide three examples of 2-D hyperchaotic maps by cascading exponential functions with the trigonometric functions. When the two bounded functions f_1 and f_2 in (1) are set to the cosine and sine functions, three 2-D hyperchaotic maps can be constructed as

$$\begin{cases} q_1(j+1) = a_1 \cos\left(\exp\left(q_2^2(j)\right)\right) \\ q_2(j+1) = a_2 \cos\left(\exp\left(q_1^2(j)\right)\right) \end{cases} \quad (2)$$

$$\begin{cases} q_1(j+1) = b_1 \sin\left(\exp\left(q_2^2(j)\right)\right) \\ q_2(j+1) = b_2 \cos\left(\exp\left(q_1^2(j)\right)\right) \end{cases} \quad (3)$$

and

$$\begin{cases} q_1(j+1) = c_1 \sin\left(\exp\left(q_2^2(j)\right)\right) \\ q_2(j+1) = c_2 \sin\left(\exp\left(q_1^2(j)\right)\right) \end{cases} \quad (4)$$

where $a_1, a_2, b_1, b_2, c_1,$ and c_2 are control parameters, respectively. The three chaotic maps are called 2-D cosine–cosine (2-D-CC) map, 2-D sine–cosine (2-D-SC) map, and 2-D sine–sine (2-D-SS) map, respectively.

The cosine and sine functions are two elementary functions with boundedness. Their outputs are within $[-1, 1]$ and do not need to be normalized, making their behaviors easily to be controlled when used to construct chaotic maps. With these properties, the cosine and sine functions are selected as representative examples to construct the three 2-D hyperchaotic maps. One has flexibility to select other bounded functions to construct new 2-D hyperchaotic maps.

C. Stability of FPs

The stability of a dynamic map can be reflected by its FPs. An FP of a function is a point that maps to itself by the function, namely $\mathbf{q}$ is an FP of f if $f(\mathbf{q}) = \mathbf{q}$. The FPs of the 2D-ECS, denoted as $(\hat{q}_1, \hat{q}_2)$, are the solutions of the 2-D equation as follows:

$$\begin{cases} \hat{q}_1 = p_1 f_1\left(\exp\left(\hat{q}_2^2\right)\right) \\ \hat{q}_2 = p_2 f_2\left(\exp\left(\hat{q}_1^2\right)\right). \end{cases}$$

When setting the f_1 and f_2 as the cosine and sine functions, one can calculate out all the FPs of the 2-D-CC map, 2-D-SC map, and 2-D-SS map under some given parameter configurations. An FP may be unstable or stable. With an unstable FP, the map's trajectories closing to the FP will be away from the FP in the sequential movement. On the contrary, if the FP is stable, the map's trajectories closing to this FP will be attracted and converge to the point. Furthermore, a locally unstable system is considered to show chaotic behaviors if all FPs are unstable. The stability of an FP can be determined by the eigenvalues of the Jacobian matrix at the point. Let $|\gamma_1|$ and $|\gamma_2|$ be two eigenvalues of the Jacobian matrix of a 2-D system. Then the FP is stable if $|\gamma_1| < 1$ and $|\gamma_2| < 1$, and it is unstable if $|\gamma_1| > 1$ or/and $|\gamma_2| > 1$. The Jacobian matrices of the 2-D-CC map, 2-D-SC map, and 2-D-SS map can be derived as

$$\begin{pmatrix} 0 & -2a_1 q_2 \exp\left(q_2^2\right) \sin\left(\exp\left(q_2^2\right)\right) \\ -2a_2 q_1 \exp\left(q_1^2\right) \sin\left(\exp\left(q_1^2\right)\right) & 0 \end{pmatrix}$$

$$\begin{pmatrix} 0 & -2b_1 q_2 \exp(q_2^2) \sin\left(\exp\left(q_2^2\right)\right) \\ 2b_2 q_1 \exp(q_1^2) \cos\left(\exp\left(q_1^2\right)\right) & 0 \end{pmatrix}$$

and

$$\begin{pmatrix} 0 & 2c_1 q_2 \exp\left(q_2^2\right) \cos\left(\exp\left(q_2^2\right)\right) \\ 2c_2 q_1 \exp\left(q_1^2\right) \cos\left(\exp\left(q_1^2\right)\right) & 0 \end{pmatrix}$$

respectively.

Because the diagonal elements of these Jacobian matrices are all zeros, the two absolute eigenvalues (AEs) $|\gamma_1|$ and $|\gamma_2|$ of each Jacobian matrix are equal, according to the rules of linear algebra. For the three maps under some parameter settings, we have calculated all the FPs and their AEs of the Jacobian matrices. Each map has many FPs and their corresponding AEs are larger than one, which means that these FPs of the three chaotic maps are unstable. Due to the space limitation, Table I only tabulates two FPs and their corresponding AEs for each map.

III. STATE-MAPPING NETWORKS

The chaos is defined in mathematical domain with infinite precision. When a chaotic system is simulated in digital domain with finite precision, chaos degradation inevitably occurs due to the precision truncation. Since all chaos-based practical applications are implemented in digital platforms, it is necessary to analyze the dynamic properties of the chaotic systems with FP arithmetic precision. The state-mapping network is a useful tool to investigate the properties of digitized chaotic maps [14], [25].

TABLE I
FPs OF THE 2-D-CC MAP, 2-D-SC MAP AND 2-D-SS MAP, AND ABSOLUTE EIGENVALUES (AEs) OF THE JACOBIAN MATRIX AT THESE FPs UNDER SOME PARAMETER SETTINGS

Parameters	2-D-SS map		2-D-SC map		2-D-CC map	
	FPs	AEs $|\gamma_{1,2}|$	FPs	AEs $|\gamma_{1,2}|$	FPs	AEs $|\gamma_{1,2}|$
$(2,3)$	$(1.9020, 2.6998)$; $(0.5836, 0.4926)$	951.9283; 3.4157	$(1.8990, 1.9137)$; $(0.4447, 1.0347)$	173.8708; 5.9941	$(1.9094, 1.7410)$; $(0.2191, 2.6010)$	123.8952; 78.5003
$(2,4)$	$(1.8991, 2.5997)$; $(0.8118, -1.4165)$	1092.9690; 130.5488	$(1.8954, 0.7997)$; $(1.1973, -1.9824)$	32.3185; 106.2162	$(1.9077, 1.4218)$; $(0.9861, 1.9087)$	83.6684; 68.2131
$(3,4)$	$(2.9000, 2.1990)$; $(1.8964, 1.2984)$	6085.1561; 21.2597	$(1.8974, 1.8031)$; $(1.8396, -1.3920)$	327.5300; 136.5217	$(1.9080, 1.6076)$; $(1.7983, 0.9570)$	229.2615; 63.8009
$(4,4)$	$(1.8984, 2.3213)$; $(0.7984, -1.2617)$	1275.0568; 23.6054	$(1.8976, 1.9086)$; $(1.8931, -1.6026)$	500.8414; 242.7408	$(1.9086, 1.9086)$; $(1.7175, 0.9962)$	512.5416; 70.2538
$\vdots$	$\vdots$	$\vdots$	$\vdots$	$\vdots$	$\vdots$	$\vdots$

In this section, we use the state-mapping network to investigate the property of the generated 2-D hyperchaotic maps in digital domain.

A state-mapping network can be generated by iterating a chaotic map in digital domain. Each possible state of the phase plane is considered as a node. The state-mapping network is generated by connecting two nodes using a directed edge, in which the former node is mapped to the latter one by the chaotic map. A state-mapping network may contain many subgraphs, and every node in the subgraph eventually converges to a cycle or a self-loop along the directed edges. All cycles of a chaotic map can be found when plotting out its related state-mapping network, and then, the dynamic characteristics, including the subgraph size and convergence time, can be presented. The subgraph size s denotes the number of nodes that are included in a subgraph, and the convergence time τ is the number of iterations required to reach to the steady state.

A. State-Mapping Network With Low Precision

When implemented using low precision, a chaotic map has a small state space, and thus, its related state-mapping network can be directly presented.

Taking the 2-D-SS map with parameters $c_1 = 5$ and $c_2 = -2$ as an example to construct the state-mapping networks. Obviously, its iterative value $q_1(j) \in [-5, 5]$ and $q_2(j) \in [-2, 2]$. When setting the arithmetic precision as $1/p$, the $q_1(j)$ has $10p$ possible states and the $q_2(j)$ has $4p$ possible states, which means that the 2-D-SS map has $40 \times p^2$ possible states. To draw the state-mapping network, we first convert each state $q = [q_1(j), q_2(j)]$ into an integer k. The conversion procedure can be mathematically expressed as follows:

$$k = F(q) = (\lfloor q_1(j) \times p \rfloor + 5p) \times 4p + (\lfloor q_2(j) \times p \rfloor + 2p)$$

where $\lfloor \cdot \rfloor$ is the floor function that returns the greatest integer that is less than or equal to " $\cdot$." The possible state can also be labeled using the ceil function or round function. However, the quantized values are slightly different when using different quantization functions, as discussed in [14]. As a result, only the floor quantization function is used in this article. Suppose that q' is the observation state outputted by the 2-D-SS map with input q. Then, $k = F(q)$ and $l = F(q')$. Finally, a directed edge from node k to node l can be generated.
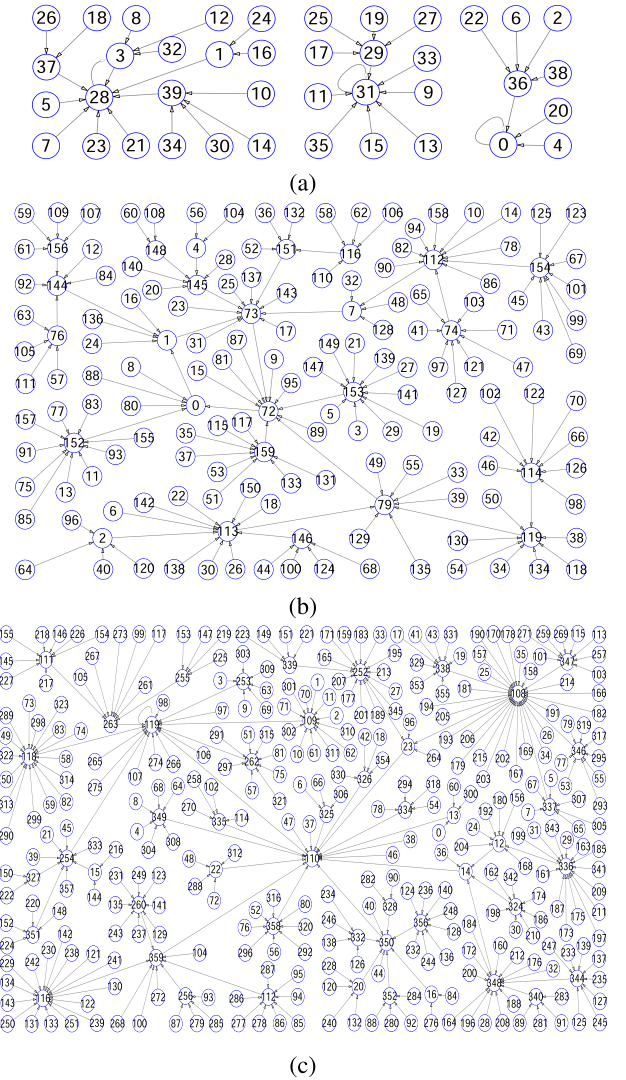

Fig. 2. State mapping networks of the 2-D-SS map under different precisions. (a) $p = 1$. (b) $p = 2$. (c) $p = 3$.

After connecting every pair of the input with its corresponding output, a state-mapping network of 2-D-SS map can be constructed.

Fig. 2 shows the state-mapping networks of the 2-D-SS map under three FP arithmetic precisions $1/p \in \{1, 1/2, 1/3\}$. One

can see that there are several evident characteristics in these state-mapping networks.

1) The whole state-mapping networks are comprised of a lot of nodes and associated weakly edges.
2) Each weakly connected node may possess multiple in-degrees but only one out-degree.
3) Each weakly connected subgraph has only one self-loop or cycle.

For each largest subgraph, there always exists an un-directed path for any pair of nodes k and l. Moreover, it can be further observed from Fig. 2(a)–(c) that the maximum convergence time τ_{max} are 2, 4, and 5, respectively, which means that the maximum convergence time increases as the FP arithmetic precision increases. More precisely, all cycles or self-loops of the 2-D-SS map under the three precisions are found. For the precision $p = 1$, two self-loops "$0 \to 0$" and "$31 \to 31$" and one period-2 cycle "$3 \to 28 \to 3$" are found in Fig. 2(a). For the precision $p = 2$, one period-4 cycle "$0 \to 1 \to 73 \to 72 \to 0$" is shown in Fig. 2(b). One self-loop "$119 \to 119$" is found in Fig. 2(c) under the precision $p = 3$. These characteristics indicate the abundant dynamic properties of the 2-D-SS map in the digital domain with low precision.

B. State-Mapping Network With High Precision

When a chaotic map is studied in digital domain with relatively high precision, it has a large state space, which makes its state-mapping networks difficult to be exhibited directly. Here, we apply a statistical approach [26] to present the dynamic characteristics of the state-mapping networks generated by the 2-D-SS map with high precision. When a state-mapping network is analyzed using statistical approach, we can obtain its cycle number n, period per, subgraph size s, mean convergence time τ_{mean}, and maximum convergence time τ_{max}. We use the parameter r to denote the ratio between the nodes of the subgraph with size s and all nodes of the network, which is equal to the probability of a randomly selected node belonging to the subgraph with size s.

In our experiment, we set the FP arithmetic precision $1/p$ as $1/2^9$, $1/2^{10}$, and $1/2^{11}$, respectively. For the three FP arithmetic precisions, the numbers of possible states generated by the proposed 2-D-SS map are 10 485 760, 41 943 040, and 167 772 160, respectively. Table II tabulates the results of the state-mapping networks under different FP arithmetic precisions. As can be seen, compared with low precision, more cycles with different periods are generated by the 2-D-SS map under high precisions. When setting the precision to $1/2^9$, $1/2^{10}$, and $1/2^{11}$, the related state-mapping networks contain 18, 41, and 32 cycles, respectively. In particular, under the precision $p = 2^{11}$, the subgraph with the maximum period cycle occupies more than 40% of the whole network from the indicator r. Moreover, for these subgraphs with the maximum period cycles, their mean convergence time τ_{mean}, maximum convergence time τ_{max}, and maximum period per increase when the precision increases. This demonstrates that the convergence time and maximum period of the 2-D-SS map can be quite large for sufficiently high precision, which is beneficial to design chaos-based industrial applications.

TABLE II
RESULTS OF STATE-MAPPING NETWORKS UNDER DIFFERENT PRECISIONS

| per	n	s	r	τ_{max}	τ_{mean}
Fixed precision $p = 2^9$					
10	13	8541430	0.8146	41	21.5327
5	2	1944282	0.1854	41	22.0915
2	1	24	$2.29 \cdot 10^{-6}$	1	0.9167
1	2	24	$2.29 \cdot 10^{-6}$	1	0.9167
Fixed precision $p = 2^{10}$					
418	1	5324861	0.1270	51	22.4438
228	1	9707554	0.2314	51	26.9463
190	1	3059451	0.0729	51	23.7950
152	1	416596	0.0099	51	19.9185
132	1	5654780	0.1348	50	23.0289
110	1	1781707	0.0425	42	18.7104
88	1	242744	0.0058	34	13.1946
60	1	3248402	0.0774	50	24.1822
40	1	139412	0.0033	42	14.3378
38	10	4376421	0.1043	51	26.4287
24	2	441920	0.0105	50	20.3756
22	6	1440382	0.0343	34	16.7389
19	1	238566	0.0057	51	28.8058
12	4	5197104	0.1239	50	27.1396
11	1	135252	0.0032	34	17.6649
10	3	429716	0.0102	42	19.5976
8	3	11424	0.0003	9	4.9184
5	1	96652	0.0023	34	20.9743
1	1	96	$2.29 \cdot 10^{-6}$	34	2.8229
Fixed precision $p = 2^{11}$					
1512	1	74329752	0.4430	140	59.7552
56	15	72229374	0.4305	45	18.5173
54	14	18439676	0.1099	140	80.3080
27	1	2773354	0.0165	140	81.2493
1	1	4	$2.38 \cdot 10^{-8}$	1	0.75
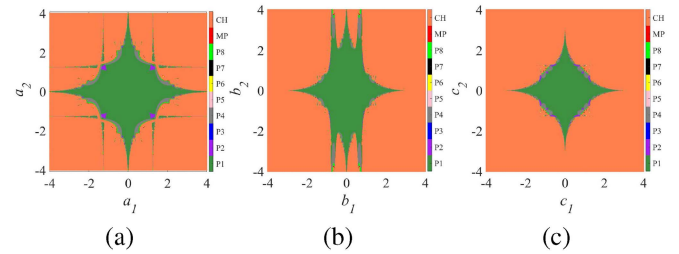
Fig. 3. Bifurcation plots of the three hyperchaotic maps in the parameter plane. (a) 2-D-CC map. (b) 2-D-SC map. (c) 2-D-SS map.

IV. HYPERCHAOTIC BEHAVIORS ANALYSIS

This section analyzes the hyperchaotic behaviors of the 2-D-CC map, 2-D-SC map and 2-D-SS map, and evaluates their performance from various indicators.

A. Hyperchaotic Behaviors

The dynamic behaviors are evaluated using the bifurcation plots. When calculating the periodicities and LEs of iterative sequences of a 2-D discrete map, a 2-D bifurcation plot with multiple colors can be portrayed in the parameter plane. Fig. 3 shows the bifurcation plots of the three maps with all parameters varying in $[-4, 4]$. In the parameter plane, each color presents each periodicity of the trajectory generated by each map with
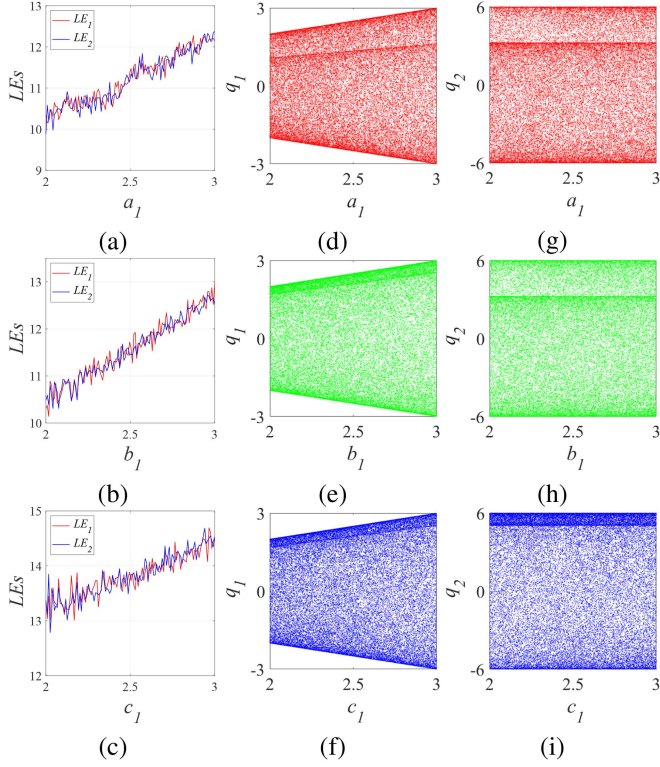
Fig. 4. Left column displays the LEs of the (a) 2-D-CC map, (b) 2-D-SC map, and (c) 2-D-SS map under the parameter ranges $a_1, b_1, c_1 \in [2, 3]$ and $a_2, b_2, c_2 = 6$, whereas the middle and right columns display the corresponding bifurcation diagrams.

corresponding parameters. The areas marked as orange and red present the chaotic behavior (labeled as CH) and multiperiod (labeled as MP), respectively, and the areas marked as other colors denote period-1 (labeled as P1) to period-8 (labeled as P8). As shown that the three maps exhibit rich dynamic behaviors, including FPs, periods, multiperiod, and chaotic behavior. To intuitively show the dynamic behaviors of the three maps, we study their bifurcation behaviors with corresponding parameters. The parameters a_1, b_1, and c_1 in the three 2-D hyperchaotic maps vary within the range [2–3], and the other parameters a_2, b_2, and c_2 are fixed as 6. Fig. 4 shows the LEs and bifurcation diagrams of the three maps. As can be seen, they have wide parameter intervals with two positive LEs, indicating a wide hyperchaotic parameter interval. Besides, the iteration variable q_1 can visit larger ranges when the parameters increase.

We also analyze the hyperchaotic sequences of the three 2-D hyperchaotic maps. The initial value and control parameter are set to $(q_1(0), q_2(0)) = (0.9, -0.2)$ and $(a_1, a_2) = (6, -6)$ for the 2-D-CC map, $(q_1(0), q_2(0)) = (0.7, 0.8)$ and $(b_1, b_2) = (2, 2)$ for the 2-D-SC map, and $(q_1(0), q_2(0)) = (0.1, 0.2)$ and $(c_1, c_2) = (5, -2)$ for the 2-D-SS map. Under these settings, the 2-D-CC map, 2-D-SC map and 2-D-SS map have two positive LEs $(LE_1, LE_2) = (19.383, 19.673)$, $(LE_1, LE_2) = (2.601, 2.610)$ and $(LE_1, LE_2) = (9.838, 9.873)$, respectively, which means that they have hyperchaotic behaviors. The trajectories of the three hyperchaotic maps are shown in Fig. 5. As
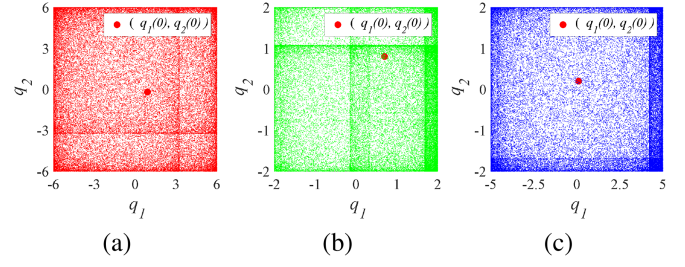

Fig. 5. Trajectories of the three hyperchaotic maps with two positive LEs the phase plane. (a) 2-D-CC map. (b) 2-D-SC map. (c) 2-D-SS map.
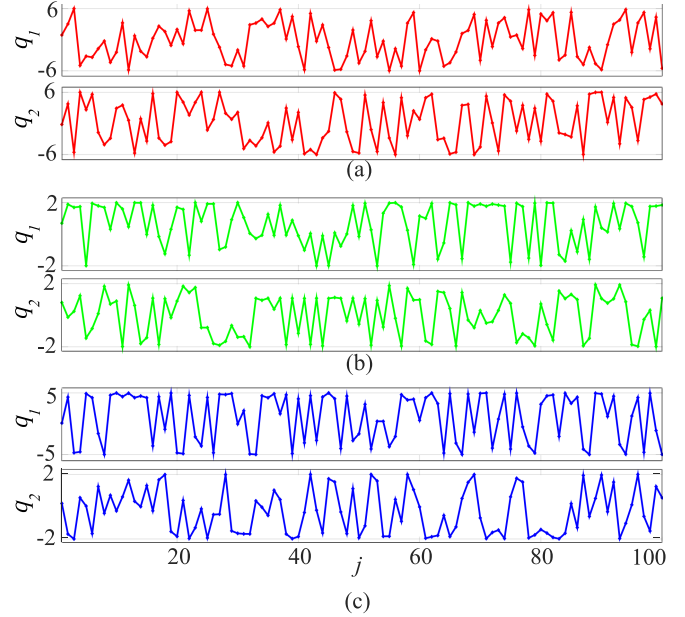

Fig. 6. Hyperchaotic sequences with 100 states. The sequences from top to bottom are generated by the 2-D-CC map, 2-D-SC map, and 2-D-SS map, respectively.

can be observed, the generated trajectories are distributed in the whole phase plane. Besides, Fig. 6 shows the six hyperchaotic sequences of these three chaotic maps. It can be seen that each sequence of the maps oscillates randomly within a certain range.

B. Performance Evaluations

We analyze the performance of the three 2-D hyperchaotic maps from the following several indicators:
1) the largest LE (LLE) [27],
2) permutation entropy (PE) [28],
3) correlation dimension (CD) [29],
4) information entropy (IE) [10], and
5) sample entropy (SE) [30].

The control parameter and initial value are set as the same values with them in Section IV-A and the lengths of the tested hyperchaotic sequences are set to 2×10^4.

Table III tabulates the experimental results of the hyperchaotic sequences generated by the three new hyperchaotic maps. As shown that the three maps have large LLE, PE,

TABLE III
PERFORMANCE INDICATORS OF THE THREE 2-D HYPERCHAOTIC MAPS

Maps	Parameters	Initials	LLE	PE	CD	IE	SE
2-D-CC map	(6,-6)	(0.9,-0.2)	19.673	0.999	1.801	6.294	1.996
2-D-SC map	(2,2)	(0.7,0.8)	2.604	0.991	1.735	5.847	1.381
2-D-SS map	(5,-2)	(0.1,0.2)	9.873	0.999	1.732	4.699	1.509

TABLE IV
COMPARING RESULTS OF THE LLE, PE, CD, IE, AND SE OF DIFFERENT
2-D MAPS

Maps	Parameters	Initials	LLE	PE	CD	IE	SE
Hénon [22]	(1.4, 0.3)	(0.3, 0.4)	0.420	0.879	1.222	4.237	0.457
Jiang et al. [24]	(1.2, 2)	(0.27, 0.28)	0.133	0.739	1.004	3.587	0.230
Li et al. [20]	(0.5, 2.33)	(1, 1)	0.268	0.897	1.518	3.649	0.524
Kong et al. [21]	3.565	(1, −2)	0.237	0.890	1.523	4.196	0.564
Bao et al. [31]	1.78	(−0.5, 0.5)	0.262	0.910	1.501	4.463	0.532
2-D-CC map	(6, −6)	(0.1, 0.2)	19.673	0.999	1.801	6.294	1.996

CD, IE, and SE values, demonstrating the complex chaotic behaviors of the proposed 2-D hyperchaotic maps. With complex chaotic behaviors, they are suitable for many chaos-based applications.

C. Performance Comparisons

To highlight the superior performance indicators of our newly generated 2-D hyperchaotic chaotic maps, we compare the performance indicators of the three 2-D chaotic maps with existing 2-D maps, including the Hénon map [22], Jiang et al. [24] map, Li et al. [20] map, Kong et al. [21] map, and Bao et al. [31] map. To provide a fair comparison, the parameters and initial values of these maps are set as the values that can make them achieve the best performance indicators.

Table IV tabulates the comparison results of the LLE, PE, CD, IE, and SE for different 2-D maps. We only show the results of our 2-D-CC map in Table IV, since the results of the other two maps can be tabulated in Table III. As can be seen, the 2-D-CC map can achieve higher LLE, PE, CD, IE, and SE values than other existing chaotic maps. The comparison results further show the high performance indicators of the hyperchaotic maps generated by our 2D-ECS.

V. HARDWARE IMPLEMENTATION AND APPLICATION

In this section, we first implement the three 2-D hyperchaotic maps generated by the 2D-ECS on a digital hardware platform, and then apply the three 2-D hyperchaotic maps to the applications of PRNG and secure communication using the hyperchaotic sequences generated by the three maps.

A. Hardware Experiment Verification

When a hyperchaotic map is applied to industrial applications, it should be implemented on the hardware platform. Here, to show the easy hardware implementation of the three 2-D hyperchaotic maps generated by the 2D-ECS, we design a
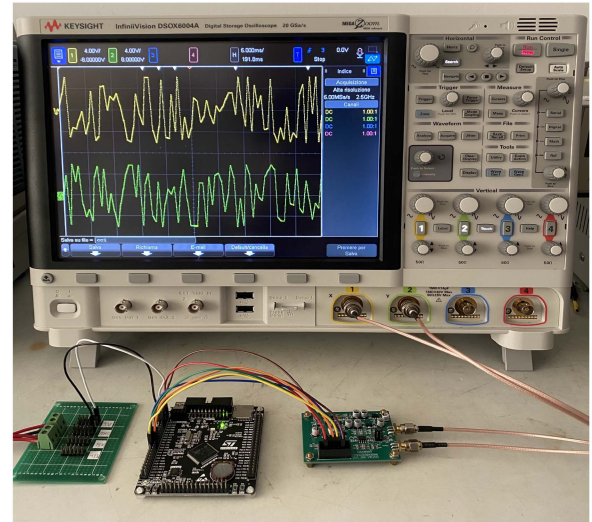

Fig. 7. Microcontroller-based hardware platform and its generated hyperchaotic sequences for the 2-D-CC map.

microcontroller-based hardware platform and use it to implement the three 2-D hyperchaotic maps.

Since the microcontroller has many properties including low cost, pony size, and ultralow power, it is widely employed in industrial applications. In our designed experiments, the experimental devices mainly contain a 32-bit high-performance microcontroller STM32F407VET6, two 12-bit D/A converters DAC8563, an oscilloscope DSO6004 A, and some peripheral-linked circuits. Fig. 7 shows the snapshot of the hardware devices. The microcontroller is used to implement the hyperchaotic maps, the D/A converters output analog voltage signals, and the oscilloscope displays the obtained results. According to the mathematical expressions of the three chaotic maps in (2)–(4), we first program the models using C language and then download the programmed codes to the microcontroller. The control parameters and initial values are set to the same values as them in Section IV-A, and they are preloaded into the hardware platform. When running the program in the microcontroller, the two-channel hyperchaotic sequences of each 2-D chaotic map can be synchronously outputted.

The outputted two-channel hyperchaotic signals of all the chaotic maps are captured from the oscilloscope and shown in Fig. 8. As shown that the three groups of two-channel chaotic sequences oscillate randomly within certain amplitude ranges. The simulation results indicate the effectiveness and feasibility of the hardware implementation for the three 2-D hyperchaotic maps.

B. Application in PRNG

Since a chaotic system has many properties, including initial state sensitivity, aperiodicity, and ergodicity, it is widely applied to PRNG. This section designs PRNGs using the three 2-D hyperchaotic maps generated by the 2D-ECS, and then tests their randomness.
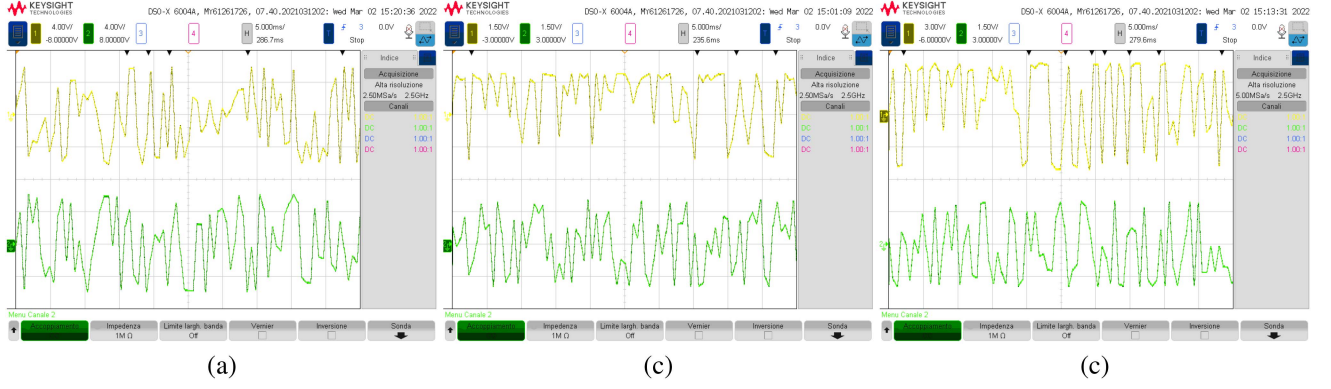
Fig. 8. Three groups of two-channel voltage sequences captured from the hardware platform for the (a) 2-D-CC map, (b) 2-D-SC map, and (c) 2-D-SS map. The top sequence is the output of q_1 and the bottom sequence is the output of q_2 in each hyperchaotic map.

TABLE V
TESTU01 TEST RESULTS OF THE PRNS GENERATED BY DIFFERENT CHAOTIC MAPS WITH TYPICAL CONTROL PARAMETERS AND INITIAL VALUES

Batteries	Length of PRNs	Hénon's [22]	Jiang's [24]	Li's [20]	Kong's [21]	Bao's [31]	2D-CC map	2-D-SC map	2-D-SS map
Rabbit	128 Gb	34/40	37/40	38/40	40/40	7/40	40/40	40/40	40/40
Alphabit	128 Gb	14/17	17/17	17/17	17/17	1/17	17/17	17/17	17/17
BlockAlphabit	128 Gb	84/102	102/102	80/102	101/102	1/102	102/102	102/102	102/102
FIPS-140-2	About19 Kb	16/16	16/16	16/16	16/16	16/16	16/16	16/16	16/16
PseudoDIEH.	About 5 Gb	126/126	126/126	126/126	125/126	126/126	126/126	126/126	126/126
SmallCrush	About 6 Gb	13/15	13/15	14/15	15/15	12/15	15/15	15/15	15/15
Crush	About 1 Tb	50/144	51/144	48/144	142/144	48/144	144/144	144/144	144/144
BigCrush	About 10 Tb	90/160	103/160	86/160	159/160	7/160	160/160	160/160	160/160

The *m/n* denotes passing *m* out of *n* statistical tests.

1) Design of PRNG: Suppose that $Q_1 = \{q_1(1), q_1(2), \ldots, q_1(j), \cdots\}$ and $Q_2 = \{q_2(1), q_2(2), \ldots, q_2(j), \cdots\}$ are two sets of chaotic sequences outputted by a 2-D chaotic map. The pseudorandom numbers (PRNs) can be generated by

$$Q = \lfloor (q_1(j) + q_2(j)) \times 10^7 \rfloor \mod 2^8 \quad (5)$$

where $\lfloor \cdot \rfloor$ is the function that returns the greatest integer that is less than or equal to " $\cdot$." It is obvious that an 8-bit stream can be obtained from each pair of the elements in Q_1 and Q_2. The designed PRNG uses two sequences as input and is suitable for chaotic maps of any dimension. When a 1-D chaotic map is used as the source chaotic map, one can use it to generate two chaotic sequences with different initial values, and then use the two chaotic sequences as the inputs of the PRNG. When an HD chaotic map is used as the source chaotic map, one can directly use its two chaotic sequences as inputs.

2) Randomness Test: Researchers developed many test standards to test the randomness of PRNs, such as the NIST SP 800-22, DIEHARD, and TestU01. To the best of our knowledge, the TestU01 standard is the strictest one and can test considerably longer random sequences than other test standards. The largest data that can be measured by the TestU01 can reach to 10 Tb. The TestU01 provides eight batteries to test the empirical statistics of the PRNs. These eight batteries are developed to find the nonrandomness area of PRNs from various aspects. Each battery is composed of a lot of statistical tests, and each statistical test can obtain a *p*-value. According to the discussions in [32], the tested PRNs are considered to pass the related statistical test if the obtained *p*-value falls into the range [0.001,0.999].

In our experiments, the initial values and parameters of the 2-D-CC map, 2-D-SC map and 2-D-SS map are set the same values as them in the performance evaluations in Section IV-A. For each competing chaotic map, its control parameters and initial values are set to the same values with them in Table IV. Since the *Rabbit*, *Alphabit*, and *BlockAlphabit* batteries can utilize different lengths of PRNs as input, the binary sequence lengths in the three test suites are fixed as 128 Gb. The other five batteries test the PRNs with default lengths, and the *BigCrush* battery contains 160 statistical tests, and its test length can approach to 10 Tb.

Table V tabulates the test results of the PRNGs using different chaotic maps. As can be observed that the PRNs generated from our 2-D hyperchaotic maps can successfully pass all the statistical tests, while some other competing PRNGs fail to pass some statistical tests. These results demonstrate that our 2-D hyperchaotic maps can produce a large number of PRNs with high randomness, which further indicates that the maps possess high complexity to resist chaos degradation.

C. Secure Communication Application

Chaotic sequence is usually used to carry secret data, due to its large bandwidth and low power density [33]. This section utilizes the reference-shifted differential chaos shift keying (RS-DCSK)
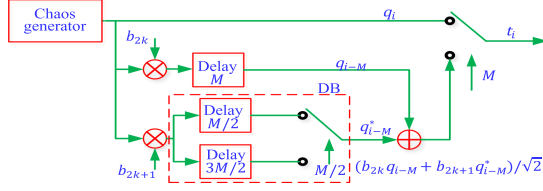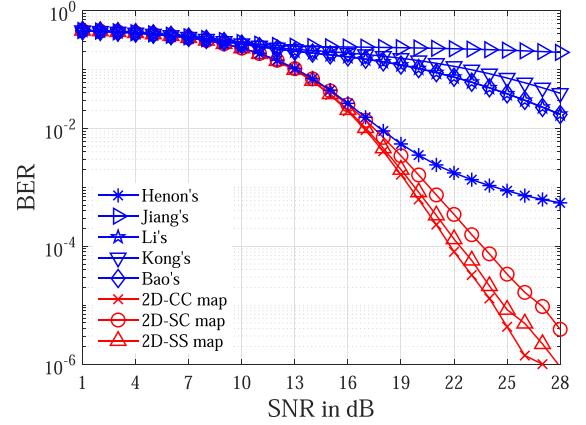
Fig. 9.   Transmitter of the RS-DCSK.

Fig. 10.   BERs of the RS-DCSK using various 2-D chaotic maps at the spread factor $M = 40$ and $SNR \in \{1, 2, \ldots, 28\}$.

proposed in [33] to test the performance of the three hyperchaotic maps in secure communication application.

1) Scheme of RS-DCSK: The RS-DCSK includes the transmitter and receiver components. The structure of the transmitter is shown in Fig. 9. The chaos generator can generate chaotic sequences with given initial conditions. The generated chaotic sequence is transmitted directly as one reference signal and its exact replica is used to modulate information bits. After switching the time, the final transmitted signal is formed. For kth frame, the reference signal $\mathbf{Q}_k = \{q_i | 2kM < i \leq (2k+1)M\}$ is an $M-$length chaotic sequence, where M is the spread factor. The mathematical expression of the kth frame in the transmitted signal can be written as follows:

$$
t_i =
\begin{cases}
q_i & 2kM < i \leq (2k+1)M \\
\frac{\sqrt{2}}{2}(b_{2k}q_{i-M} + b_{2k+1}q_{i-\frac{M}{2}}) & (2k+1)M < i \leq 2kM + \frac{3}{2}M. \\
\frac{\sqrt{2}}{2}(b_{2k}q_{i-M} + b_{2k+1}q_{i-\frac{3M}{2}}) & 2kM + \frac{3}{2}M < i \leq 2(k+1)M
\end{cases}
$$

(6)

The final transmitted signal contains two components. The first component is the reference signal $\mathbf{Q}_k$, whereas the second component is the sum of two parts. The first part is the product of information bit b_{2k} and reference signal $\mathbf{Q}_k$, and the second part is the product of b_{2k+1} and $\mathbf{Q}_k^*$, where $\mathbf{Q}_k^*$ is generated by swapping the positions of the first and second halves of the sequence $\mathbf{Q}_k$. Thus, one frame can carry two information bits. Since the transmitter modulates the information in a continuous way, three delay blocks are required when modulating two information bits in one frame.

The receiver demodulates the transmitted signal from the transmitter. Since many physical transmission channels are noisy channels, the signal r_i may be different with the transmitted signal t_i, and thus, $r_i = t_i + \zeta_i$, where ζ_i denotes the noise part. The correlators Z_{2k} and Z_{2k+1} for the information bits b_{2k} and b_{2k+1} are calculated by adding the multiplication of r_i with its delay version r_{i-M} and r_{i-M}^*, respectively. Namely, the correlators Z_{2k} and Z_{2k+1} are written as

$$
Z_{2k} = \sum_{i=(2k+1)M+1}^{2(k+1)M} r_i r_{i-M}
$$

$$
= \frac{\sqrt{2}}{2} \sum_{i=(2k+1)M+1}^{2(k+1)M} b_{2k} q_{i-M}^2 + \psi
$$

(7)

$$
Z_{2k+1} = \sum_{i=(2k+1)M+1}^{2(k+1)M} r_i r_{i-M}^*
$$

$$
= \frac{\sqrt{2}}{2} \sum_{i=(2k+1)M+1}^{2(k+1)M} b_{2k+1} q_{i-M}^2 + \eta
$$

(8)

where ψ and η are noise parts. Since the noise has considerably smaller energy than the information bits, the signs of Z_{2k} and Z_{2k+1} are determined by the signs of the data bits b_{2k} and b_{2k+1}, respectively. Thus, despite the noise influences, the information bits can be demodulated by

$$
b_n =
\begin{cases}
1, & \text{for } Z_n > 0 \\
-1, & \text{for } Z_n < 0.
\end{cases}
$$

2) Simulation Results: Our experiments use the three new hyperchaotic maps as chaotic generators to measure the performance of the RS-DCSK in resisting transmitted noise. Since the addition white Gaussian noise (AWGN) is one of the most common noises in transmission channels, we simulate the RS-DCSK in the AWGN environment, and calculate the bit error rates (BERs) of the RS-DCSK. The parameters and initial values of the proposed chaotic maps and other competing maps are set to be the same as those in Tables III and IV, respectively.

The experiments are performed against various noise levels by fixing the spread factor $M = 40$. For each 2-D chaotic map, we randomly produce one 10^6-length bit binary, and then, calculate the BERs between the decoded information bits and original information bits, respectively, with the signal–noise-ratios (SNRs) $SNR \in \{1, 2, \ldots, 28\}$. Fig. 10 shows the BERs of RS-DCSK using different 2-D chaotic maps. As can be seen, when using the new 2-D chaotic maps as chaos generators, the RS-DCSK can always achieve smaller BERs than when using other 2-D chaotic maps as chaos generators. This result demonstrates that the chaotic maps produced by the 2D-ECS can show stronger ability to resist the AWGN than existing maps in RS-DCSK scheme.

VI. Conclusion

In this article, we proposed a 2D-ECS. The 2D-ECS could generate a large number of 2-D hyperchaotic maps by cascading exponential nonlinearity with bounded functions. To demonstrate the effects of the 2D-ECS, three 2-D hyperchaotic maps were generated by cascading the exponential functions with trigonometric functions. We analyzed the fundamental dynamic characteristics of one 2-D hyperchaotic map as an example using state-mapping networks. Property analysis disclosed that these 2-D hyperchaotic maps possessed complex dynamics and hyperchaotic behaviors. Performance evaluations showed that they had better performance indicators than existing 2-D chaotic maps. We simulated the three 2-D hyperchaotic in the hardware platform and employed their hyperchaotic sequences to design PRNGs. The test results indicated the high randomness of the generated PRNs. Finally, we employed the three new chaotic maps to secure communication, and the experimental results showed that these maps exhibit better performance in withdrawing channel noise than existing maps. Since the hyperchaotic maps generated by our 2D-ECS had high complexity, and they were suitable for many chaos-based applications. Our future work will study the applications of these 2-D hyperchaotic maps in secure video communication and image encryption.

References

[1] X. Li, J. He, C. Wen, and X.-K. Liu, "Backstepping-based adaptive control of a class of uncertain incommensurate fractional-order nonlinear systems with external disturbance," *IEEE Trans. Ind. Electron.*, vol. 69, no. 4, pp. 4087–4095, Apr. 2022.

[2] Y. Zhang and K. Li, "Successive lag synchronization on nonlinear dynamical networks via aperiodically intermittent control," *Nonlinear Dyn.*, vol. 95, no. 4, pp. 3075–3089, 2019.

[3] H. Lin et al., "An extremely simple multiwing chaotic system: Dynamics analysis, encryption application, and hardware implementation," *IEEE Trans. Ind. Electron.*, vol. 68, no. 12, pp. 12708–12719, Dec. 2021.

[4] L. Tang and J. Zhao, "Switched threshold-based fault detection for switched nonlinear systems with its application to Chua's circuit system," *IEEE Trans. Circuits Syst. I., Reg. Papers*, vol. 66, no. 2, pp. 733–741, Feb. 2019.

[5] H. G. Schuster and W. Just, *Deterministic Chaos: An Introduction*. Hoboken, NJ, USA: Wiley, 2006.

[6] R. L. Devaney, *An Introduction to Chaotic Dynamical Systems*, 2nd ed. Boulder, CO, USA: Westview Press, 2003.

[7] S. Zhang, C. Li, J. Zheng, X. Wang, Z. Zeng, and X. Peng, "Generating any number of initial offset-boosted coexisting Chua's double-scroll attractors via piecewise-nonlinear memristor," *IEEE Trans. Ind. Electron.*, vol. 69, no. 7, pp. 7202–7212, Jul. 2022.

[8] Z. Hua, Z. Zhu, Y. Chen, and Y. Li, "Color image encryption using orthogonal latin squares and a new 2D chaotic system," *Nonlinear Dyn.*, vol. 104, pp. 4505–4522, 2021.

[9] N. T. Nguyen, T. Bui, G. Gagnon, P. Giard, and G. Kaddoum, "Designing a pseudorandom bit generator with a novel five-dimensional-hyperchaotic system," *IEEE Trans. Ind. Electron.*, vol. 69, no. 6, pp. 6101–6110, Jun. 2022.

[10] Z. Hua, Y. Zhang, H. Bao, H. Huang, and Y. Zhou, "n-dimensional polynomial chaotic system with applications," *IEEE Trans. Circuits Syst. I., Reg. Papers*, vol. 69, no. 2, pp. 784–797, Feb. 2022.

[11] Y. Zhang, Z. Hua, H. Bao, H. Huang, and Y. Zhou, "An n-dimensional chaotic system generation method using parametric pascal matrix," *IEEE Trans. Ind. Informat.*, early access, Feb. 16, 2022, doi: 10.1109/TII.2022.3151984.

[12] Z. Hua, Y. Zhou, and B. Bao, "Two-dimensional sine chaotification system with hardware implementation," *IEEE Trans. Ind. Inform.*, vol. 16, no. 2, pp. 887–897, Feb. 2020.

[13] C. Fan, Q. Ding, and C. K. Tse, "Counteracting the dynamical degradation of digital chaos by applying stochastic jump of chaotic orbits," *Int. J. Bifurcation Chaos*, vol. 29, no. 08, 2019, Art. no. 1930023.

[14] C. Li, B. Feng, S. Li, J. Kurths, and G. Chen, "Dynamic analysis of digital chaotic maps via state-mapping networks," *IEEE Trans. Circuits Syst. I*, vol. 66, no. 6, pp. 2322–2335, Jun. 2019.

[15] O. Abedinia, M. Lotfi, M. Bagheri, B. Sobhani, M. Shafie-khah, and J. P. Catalao, "Improved EMD-based complex prediction model for wind power forecasting," *IEEE Trans. Sustain. Energy*, vol. 11, no. 4, pp. 2790–2802, Oct. 2020.

[16] M. Liu, S. Zhang, Z. Fan, S. Zheng, and W. Sheng, "Exponential H_∞ synchronization and state estimation for chaotic systems via a unified model," *IEEE Trans. Neural Netw. Learn. Syst.*, vol. 24, no. 7, pp. 1114–1126, Jul. 2013.

[17] S. Ergün, "On the security of chaos based "true" random number generators," *IEICE Trans. Fundam. Electron., Commun. Comput. Sci.*, vol. 99, no. 1, pp. 363–369, 2016.

[18] S. Chen, S. Yu, J. Lü, G. Chen, and J. He, "Design and FPGA-based realization of a chaotic secure video communication system," *IEEE Trans. Circuits Syst. Video Technol.*, vol. 28, no. 9, pp. 2359–2371, Sep. 2018.

[19] B. Bao, K. Rong, H. Li, K. Li, Z. Hua, and X. Zhang, "Memristor-coupled logistic hyperchaotic map," *IEEE Trans. Circuits Syst. II, Exp. Briefs*, vol. 68, no. 8, pp. 2992–2996, Aug. 2021.

[20] H. Li, Z. Hua, H. Bao, L. Zhu, M. Chen, and B. Bao, "Two-dimensional memristive hyperchaotic maps and application in secure communication," *IEEE Trans. Ind. Electron.*, vol. 68, no. 10, pp. 9931–9940, Oct. 2021.

[21] S. Kong, C. Li, H. Jiang, Q. Lai, and X. Jiang, "A 2D hyperchaotic map with conditional symmetry and attractor growth," *Chaos*, vol. 31, no. 4, 2021, Art. no. 043121.

[22] M. Hénon, "A two-dimensional mapping with a strange attractor," in *The Theory of Chaotic Attractors*. Berlin, Germany: Springer, 1976, pp. 94–102.

[23] J. C. Panahi, S. Sprott,, and S. Jafari, "Two simplest quadratic chaotic maps without equilibrium," *Int. J. Bifurcation Chaos*, vol. 28, no. 12, 2018, Art. no. 1850144.

[24] H. Jiang, Y. Liu, Z. Wei, and L. Zhang, "A new class of two-dimensional chaotic maps with closed curve fixed points," *Int. J. Bifurcation Chaos*, vol. 29, no. 7, 2019, Art. no. 1950094.

[25] C. Li, K. Tan, B. Feng, and J. Lu, "The graph structure of the generalized discrete arnold's cat map," *IEEE Trans. Comput.*, vol. 71, no. 2, pp. 364–377, Feb. 2022.

[26] Z. Galias, "Periodic orbits of the logistic map in single and double precision implementations," *IEEE Trans. Circuits Syst. II, Exp. Briefs*, vol. 68, no. 11, pp. 3471–3475, Nov. 2021.

[27] C. Shen, S. Yu, J. Lü, and G. Chen, "Constructing hyperchaotic systems at will," *Int. J. Circuit Theory Appl.*, vol. 43, no. 12, pp. 2039–2056, 2015.

[28] Y. Cao, W.-W. Tung, J. Gao, V. A. Protopopescu, and L. M. Hively, "Detecting dynamical changes in time series using the permutation entropy," *Phys. Rev. E*, vol. 70, no. 4, 2004, Art. no. 046217.

[29] L. Lacasa and J. Gómez-Gardeñes, "Correlation dimension of complex networks," *Phys. Rev. Lett.*, vol. 110, no. 16, 2013, Art. no. 168703.

[30] J. S. Richman and J. R. Moorman, "Physiological time-series analysis using approximate entropy and sample entropy," *Amer. J. Physiol.-Heart Circulatory Physiol.*, vol. 278, no. 6, pp. 2039–2049, 2000.

[31] H. Bao, Z. Hua, H. Li, M. Chen, and B. Bao, "Discrete memristor hyperchaotic maps," *IEEE Trans. Circuits Syst. I., Reg. Papers*, vol. 68, no. 11, pp. 4534–4544, Nov. 2021.

[32] P. L'Ecuyer and R. Simard, "Testu01: AC library for empirical testing of random number generators," *ACM Trans. Math. Softw.*, vol. 33, no. 4, pp. 1–40, 2007.

[33] H. Yang, G. Jiang, L. Xia, and X. Tu, "Reference-shifted DCSK modulation scheme for secure communication," in *Proc. Int. Conf. Comput. Netw. Commun.*, 2017, pp. 1073–1076.

Yinxing Zhang received the M.S. degree in fundamental mathematics from the Guilin University of Electronic Technology, Guilin, China, in 2019. He is currently working toward the Ph.D. degree in computer science and technology with the School of Computer Science and Technology, Harbin Institute of Technology, Shenzhen, China.

His current research interests include chaotic system and nonlinear system control.

Han Bao (Member, IEEE) received the B.S. degree in landscape design from the Jiangxi University of Finance and Economics, Nanchang, China, in 2015, the M.S. degree in art and design from Changzhou University, Changzhou, China, in 2018, and the Ph.D. degree in nonlinear system analysis and measurement technology from the Nanjing University of Aeronautics and Astronautics, Nanjing, China, in 2021.

In 2019, he visited Computer Science Department, University of Auckland, Auckland, New Zealand. He is currently a Lecturer with the School of Microelectronics and Control Engineering, Changzhou University, Changzhou, China. His research interests include memristive neuromorphic circuit, nonlinear circuits and systems, and artificial intelligence.

Zhongyun Hua (Member, IEEE) received the B.S. degree in software engineering from Chongqing University, Chongqing, China, in 2011, and the M.S. and Ph.D. degrees in software engineering from University of Macau, Macau, China, in 2013 and 2016, respectively.

He is currently an Associate Professor with the School of Computer Science and Technology, Harbin Institute of Technology, Shenzhen, China. He has authored or coauthored more than six papers on the subject, receiving more than 3800 citations. His research interests include chaotic system, chaos-based applications, and multimedia security.

He is currently an Associate Editor for the *International Journal of Bifurcation and Chaos*.

Hejiao Huang received the Ph.D. degree in computer science from the City University of Hong Kong, Hong Kong, in 2004 .

She was an Invited Professor with the National Institute for Research in Digital Science and Technology, Bordeaux, France. She is currently a Professor with the Harbin Institute of Technology, Shenzhen, China. Her research interests include cloud computing, network security, trustworthy computing, and formal methods for system design and wireless networks.